
Volume 93, Issue 12, November 2011
ISSN: 0263-8223
ELSEVIER
COMPOSITE STRUCTURES
EDITOR: A. J. M. FERREIRA

Composite Structures 93 (2011) 3252–3261

Contents lists available at ScienceDirect

Composite Structures

journal homepage: www.elsevier.com/locate/compstruct

Higher order shear deformation effects on analysis of laminates with piezoelectric fibre reinforced composite actuators

S.M. Shiyekar [a,*], Tarun Kant [b]

[a] Department of Civil Engineering, Sinhgad College of Engineering, Vadgaon (Bk), Pune 411 041, India
[b] Department of Civil Engineering, Indian Institute of Technology Bombay, Powai, Mumbai 400 076, India

ARTICLE INFO

Article history:
Available online 24 May 2011

Keywords:
Higher order theory
Piezoelectric fiber reinforced composites (PFRC)
Laminates

ABSTRACT

A complete analytical solution for cross-ply composite laminates integrated with piezoelectric fiber-reinforced composite (PFRC) actuators under bi-directional bending is presented in this paper. A higher order shear and normal deformation theory (HOSNT12) is used to analyze such hybrid or smart laminates subjected to electromechanical loading. The displacement function of the present model is approximated by employing Taylor's series in the thickness coordinate, while the electro-static potential is assumed to be layer wise (LW) linear through the thickness of PFRC. The equations of equilibrium are obtained using principle of minimum potential energy and solution is by Navier's technique. Transverse shear stresses are presented at the interface of PFRC actuator and laminate under the action of electrostatic potentials. Results are compared with first order shear deformation theory (FOST) and exact solution.

1. Introduction

Piezoelectric materials transform elastic field into the electric field and converse behavior leads many researchers to study their controlling capabilities applicable to structures like laminated plates and shells. Such laminates are called smart, intelligent, adaptive as well as hybrid.

Piezoelectric materials show coupling phenomenon between elastic and electric fields. Tiersten and Mindlin [1] initiated work on piezoelectric plates. Tiersten [2] contributed further by establishing the governing equations of linear piezoelectric continuum by studying vibrations of a single piezoelectric layer.

Mallik and Ray [3] proposed the concept of unidirectional piezoelectric fiber reinforced composite (PFRC) materials and presented their effective elastic and piezoelectric properties using micromechanical analysis. Piezoelectric stress/strain coefficients of PFRC are improved considerably as compared to monolithic piezoelectric materials.

Many investigators [4–11] studied hybrid laminates using various plate theories viz. *equivalent single layer* (ESL), *layer wise* (LW), *zigzag* and *discrete layer theories* (DLT) and also analytical solution using FOST [11]. Here in this paper a complete and simple analytical solution is discussed using a higher order shear and normal deformation theory.

Ray et al. [12] developed three dimensional (3D) elasticity solutions for an intelligent plate simply supported and perfectly bonded with distributed *polyvinylidene fluoride* (PVDF) piezoelectric layers at top and bottom and presented static displacement control of laminates for various span to depth ratios. Further Mallik and Ray [13,14] presented exact and *finite element* (FE) solutions for PFRC activated laminated composites respectively. Heyliger [15] obtained exact solution for an unsymmetric cross ply composite laminate attached with PZT-4 layers of piezoelectric material at upper and lower surfaces. Vel and Batra [16] used Eshelby-Stroh formulation to obtained 3D elasticity solution to analyze multilayered piezoelectric plate with arbitrary boundary conditions.

Initially Kant [17] developed complete set of variationally consistent governing equations of equilibrium and presented first FE model based on higher order shear deformation theory (HOST) [18]. Pandya and Kant [19] and Kant and Manjunatha [20] extended the HOST for symmetric and unsymmetric laminates. Further Kant and Swaminathan [21] presented a refined higher order model and discussed analytical solution for sandwiches and laminates. In this present paper, ESL based HOSNT12 is used to model elastic quantities where as electrostatic potential is by LW approach. Transverse shear and normal stresses are evaluated by using equations of equilibrium of elasticity. It is believed that HOSNT12 will give accurate predictions of displacements and stresses. Further, a linear function for electrostatic potential through actuating layer is considered sufficient in view of its small thickness compared to that of the composite laminate.

* Corresponding author. Tel.: +91 20 2410 0000; fax: +91 20 2435 4721.
E-mail address: smshiyekar.scoe@sinhgad.edu (S.M. Shiyekar).

0263-8223/$ - see front matter
doi:10.1016/j.compstruct.2011.05.016

2. Formulation

2.1. Displacement function

Bidirectional flexure analysis of all side simply supported cross ply laminate attached with PFRC actuator at top is considered (Fig. 1). Span of the hybrid laminate is a along x-axis and b along y-axis. Thickness of elastic substrate is h which is along z-axis located at $-h/2$ and $+h/2$ from bottom and top of the composite cross-ply laminate respectively while, thickness of PFRC actuator is t_p.

Displacement components $u(x,y,z)$, $v(x,y,z)$ and $w(x,y,z)$ at any point in the laminate are expanded in powers of z-axis to approximate three dimensional (3D) elasticity problem as a two dimensional (2D) laminated plate problem. The assumed displacement field is in the following form.

Model HOSNT12: [21]

$$\begin{aligned}
u(x,y,z) &= u_0(x,y) + z\theta_x(x,y) + z^2u_0^*(x,y) + z^3\theta_x^*(x,y),\\
v(x,y,z) &= v_0(x,y) + z\theta_y(x,y) + z^2v_0^*(x,y) + z^3\theta_y^*(x,y),\\
w(x,y,z) &= w_0(x,y) + z\theta_z(x,y) + z^2w_0^*(x,y) + z^3\theta_z^*(x,y),
\end{aligned} \tag{1}$$

where the parameters u_0, v_0 are in-plane displacements and w_0 is transverse displacement at any point (x,y) on the mid-plane of the laminate. θ_x and θ_y are rotations of normal to mid-plane about y and x axes respectively. Other parameters such as u_0^*, θ_x^*, v_0^*, θ_y^*, w_0^*, θ_z, θ_z^* are the corresponding higher order terms defined at mid-plane. Mid-plane strain displacement relation can be derived utilizing the following elasticity relations.

$$\begin{Bmatrix}\varepsilon_x\\ \varepsilon_y\\ \varepsilon_z\\ \gamma_{xy}\\ \gamma_{yz}\\ \gamma_{xz}\end{Bmatrix} = \left\{\frac{\partial u}{\partial x} \quad \frac{\partial v}{\partial y} \quad \frac{\partial w}{\partial z} \quad \frac{\partial u}{\partial y}+\frac{\partial v}{\partial x} \quad \frac{\partial v}{\partial z}+\frac{\partial w}{\partial y} \quad \frac{\partial u}{\partial z}+\frac{\partial w}{\partial x}\right\}^t. \tag{2}$$

2.2. Coupled constitutive relationships and stress resultants

Linear constitutive equation which couples the elastic and electric field for a single piezoelectric layer are [2].

$$\begin{aligned}
\{\sigma\} &= [Q]\{\varepsilon\} - [e]\{E\},\\
\{D\} &= [e]^t\{\varepsilon\} + [\eta]\{E\}.
\end{aligned} \tag{3}$$

The electric field intensity vector E related to electrostatic potential $\xi(x,y,z)$ in the L^{th} layer is given by

$$E_x^L = -\frac{\partial\xi(x,y,z)^L}{\partial x}, \qquad E_y^L = -\frac{\partial\xi(x,y,z)^L}{\partial y}, \qquad E_z^L = -\frac{\partial\xi(x,y,z)^L}{\partial z}, \tag{4}$$

where σ, Q, ε, e, E, D and η are, stress vector, elastic constant matrix, strain vector, piezoelectric constant matrix, electric field intensity vector, electric displacement vector and dielectric constant matrix respectively. Effective piezoelectric constant matrix e and dielectric matrix η for PFRC layer are given as [13,14].

$$[e] = \begin{bmatrix} 0 & 0 & e_{31}\\ 0 & 0 & e_{32}\\ 0 & 0 & e_{33}\\ 0 & 0 & 0\\ 0 & e_{24} & 0\\ e_{15} & 0 & 0 \end{bmatrix}, \qquad [\eta] = \begin{bmatrix} \eta_{11} & 0 & 0\\ 0 & \eta_{22} & 0\\ 0 & 0 & \eta_{33} \end{bmatrix}. \tag{5}$$

First set of Eq. 3 can be presented in two components of stresses. One is elastic stress component (es) and other is piezoelectric stress component (pz) and written as

$$\{\sigma\} = \{\sigma\}^{es} - \{\sigma\}^{pz}, \tag{6}$$

where

$$\{\sigma\}^{es} = \begin{bmatrix} Q_{11} & Q_{12} & Q_{13} & Q_{14} & 0 & 0\\ Q_{12} & Q_{22} & Q_{23} & Q_{24} & 0 & 0\\ Q_{13} & Q_{23} & Q_{33} & Q_{34} & 0 & 0\\ Q_{14} & Q_{24} & Q_{34} & Q_{44} & 0 & 0\\ 0 & 0 & 0 & 0 & Q_{55} & Q_{56}\\ 0 & 0 & 0 & 0 & Q_{56} & Q_{66} \end{bmatrix}^L \begin{Bmatrix}\varepsilon_x\\ \varepsilon_y\\ \varepsilon_z\\ \gamma_{xy}\\ \gamma_{yz}\\ \gamma_{xz}\end{Bmatrix},$$

$$\{\sigma\}^{pz} = \begin{bmatrix} 0 & 0 & e_{31}\\ 0 & 0 & e_{32}\\ 0 & 0 & e_{33}\\ 0 & 0 & 0\\ 0 & e_{24} & 0\\ e_{15} & 0 & 0 \end{bmatrix}^L \begin{Bmatrix} -\frac{\partial\xi(x,y,z)}{\partial x}\\ -\frac{\partial\xi(x,y,z)}{\partial y}\\ -\frac{\partial\xi(x,y,z)}{\partial z} \end{Bmatrix}^L, \tag{7}$$

and Q_{ij} are the transformed elastic constants with respect to the x, y and z axes of the elastic laminate. Stress resultants are also defined as elastic and piezoelectric stress resultants as *Elastic stress resultants* $[Q\,S\,M\,N]^{es}$:

$$\left[Q_x^{es}, Q_y^{es} | Q_x^{es^*}, Q_y^{es^*}\right] = \sum_{L=1}^{n} \int_{Z_L}^{Z_{(L+1)}} \left\{\tau_{xz}^{es}, \tau_{yz}^{es}\right\}[1|z^2]\,dz,$$

$$\left[S_x^{es}, S_y^{es} | S_x^{es^*}, S_y^{es^*}\right] = \sum_{L=1}^{n} \int_{Z_L}^{Z_{(L+1)}} \left\{\tau_{xz}^{es}, \tau_{yz}^{es}\right\}[z|z^3]\,dz,$$

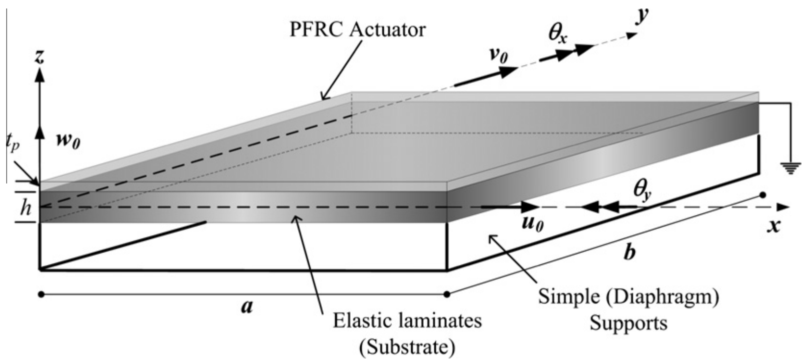

Fig. 1. Geometry of elastic substrate simply (diaphragm) supported along all edges attached with PFRC actuator at top.

$$\left[M_x^{es}, M_y^{es}, M_{xy}^{es} \middle| M_x^{es^*}, M_y^{es^*}, M_{xy}^{es^*}\right] = \sum_{L=1}^{n} \int_{Z_L}^{Z_{(L+1)}} \left\{\sigma_x^{es}, \sigma_y^{es}, \tau_{xy}^{es}\right\}[z|z^3]\, dz,$$

$$M_z^{es} = \sum_{L=1}^{n} \int_{Z_L}^{Z_{(L+1)}} z\sigma_z^{es}\, dz,$$

$$\left[N_x^{es}, N_y^{es}, N_z^{es}, N_{xy}^{es} \middle| N_x^{es^*}, N_y^{es^*}, N_z^{es^*}, N_{xy}^{es^*}\right] = \sum_{L=1}^{n} \int_{Z_L}^{Z_{(L+1)}} \left\{\sigma_x^{es}, \sigma_y^{es}, \sigma_z^{es}, \tau_{xy}^{es}\right\}[1|z^2]\, dz. \tag{8}$$

Piezoelectric stress resultants $[Q\,S\,M\,N]^{pz}$:

$$\left[Q_x^{pz}, Q_y^{pz} | Q_x^{pz^*}, Q_y^{pz^*}\right] = \int_{+h/2}^{h/2+tp} \left\{\tau_{xz}^{pz}, \tau_{yz}^{pz}\right\}[1|z^2]\, dz,$$

$$\left[S_x^{pz}, S_y^{pz} | S_x^{pz^*}, S_y^{pz^*}\right] = \int_{+h/2}^{h/2+tp} \left\{\tau_{xz}^{pz}, \tau_{yz}^{pz}\right\}[z|z^3]\, dz,$$

$$\left[M_x^{pz}, M_y^{pz}, M_{xy}^{pz} | M_x^{pz^*}, M_y^{pz^*}, M_{xy}^{pz^*}\right] = \int_{+h/2}^{h/2+tp} \left\{\sigma_x^{pz}, \sigma_y^{pz}, \tau_{xy}^{pz}\right\}[z|z^3]\, dz,$$

$$M_z^{pz} = \int_{+h/2}^{h/2+tp} z\sigma_z^{pz}\, dz,$$

$$\left[N_x^{pz}, N_y^{pz}, N_z^{pz}, N_{xy}^{pz} | N_x^{pz^*}, N_y^{pz^*}, N_z^{pz^*}, N_{xy}^{pz^*}\right] = \int_{+h/2}^{h/2+tp} \left\{\sigma_x^{pz}, \sigma_y^{pz}, \sigma_z^{pz}, \tau_{xy}^{pz}\right\}[1|z^2]\, dz. \tag{9}$$

Total stress resultants$[Q\ S\ M\ N]$

$$= [Q\ S\ M\ N]^{es} + [Q\ S\ M\ N]^{pz}. \tag{10}$$

Governing equations of equilibrium: [21]

Using principle of minimum potential energy, the equations of equilibrium are obtained as

$$\begin{aligned}
&\delta u_0 : \tfrac{\partial N_x}{\partial x} + \tfrac{\partial N_{xy}}{\partial y} = 0 && \delta u_0^* : \tfrac{\partial N_x^*}{\partial x} + \tfrac{\partial N_{xy}^*}{\partial y} - 2S_x = 0\\
&\delta v_0 : \tfrac{\partial N_y}{\partial y} + \tfrac{\partial N_{xy}}{\partial x} = 0 && \delta v_0^* : \tfrac{\partial N_y^*}{\partial y} + \tfrac{\partial N_{xy}^*}{\partial x} - 2S_y = 0\\
&\delta w_0 : \tfrac{\partial Q_x}{\partial x} + \tfrac{\partial Q_y}{\partial y} + (q_z^+) = 0 && \delta w_0^* : \tfrac{\partial Q_x^*}{\partial x} + \tfrac{\partial Q_y^*}{\partial y} - 2M_z^* + \tfrac{h^2}{4}(q_z^+) = 0\\
&\delta \theta_x : \tfrac{\partial M_x}{\partial x} + \tfrac{\partial M_{xy}}{\partial y} - Q_x = 0 && \delta \theta_x^* : \tfrac{\partial M_x^*}{\partial x} + \tfrac{\partial M_{xy}^*}{\partial y} - 3Q_x^* = 0\\
&\delta \theta_y : \tfrac{\partial M_y}{\partial y} + \tfrac{\partial M_{xy}}{\partial x} - Q_y = 0 && \delta \theta_y^* : \tfrac{\partial M_y^*}{\partial y} + \tfrac{\partial M_{xy}^*}{\partial x} - 3Q_y^* = 0\\
&\delta \theta_z : \tfrac{\partial S_x}{\partial x} + \tfrac{\partial S_y}{\partial y} - N_z + \tfrac{h}{2}(q_z^+) = 0 && \delta \theta_z^* : \tfrac{\partial S_x^*}{\partial x} + \tfrac{\partial S_y^*}{\partial y} - 3N_z^* + \tfrac{h^3}{8}(q_z^+) = 0.
\end{aligned} \tag{11}$$

Following are the mechanical and electrical in-plan boundary conditions used for simply supported plate

At edges $x = 0$ and $x = a$:

$$v_0 = 0,\ w_0 = 0,\ \theta_y = 0,\ \theta_z = 0,\ M_x = 0,\ N_x = 0,\ v_0^* = 0,$$
$$w_0^* = 0,\ \theta_y^* = 0,\ \theta_z^* = 0,\ M_x^* = 0,\ N_x^* = 0,\ \xi = 0.$$

At edges $y = 0$ and $y = b$:

$$u_0 = 0,\ w_0 = 0,\ \theta_x = 0,\ \theta_z = 0,\ M_y = 0,\ N_y = 0,\ u_0^* = 0,$$
$$w_0^* = 0,\ \theta_x^* = 0,\ \theta_z^* = 0,\ M_y^* = 0,\ N_y^* = 0,\ \xi = 0.$$

In Navier's solution procedure the load, electric potential and mid-plane displacements are expanded as follows, satisfying the above boundary conditions.

$$\begin{aligned}
u_0 &= \sum_{m=1,3,5}^{\infty} \sum_{n=1,3,5}^{\infty} u_{0_{mn}} \cos\left(\tfrac{m\pi x}{a}\right) \sin\left(\tfrac{n\pi y}{b}\right)\\
u_0^* &= \sum_{m=1,3,5}^{\infty} \sum_{n=1,3,5}^{\infty} u_{0_{mn}}^* \cos\left(\tfrac{m\pi x}{a}\right) \sin\left(\tfrac{n\pi y}{b}\right)\\
v_0 &= \sum_{m=1,3,5}^{\infty} \sum_{n=1,3,5}^{\infty} v_{0_{mn}} \sin\left(\tfrac{m\pi x}{a}\right) \cos\left(\tfrac{n\pi y}{b}\right)\\
v_0^* &= \sum_{m=1,3,5}^{\infty} \sum_{n=1,3,5}^{\infty} v_{0_{mn}}^* \sin\left(\tfrac{m\pi x}{a}\right) \cos\left(\tfrac{n\pi y}{b}\right)\\
w_0 &= \sum_{m=1,3,5}^{\infty} \sum_{n=1,3,5}^{\infty} w_{0_{mn}} \sin\left(\tfrac{m\pi x}{a}\right) \sin\left(\tfrac{n\pi y}{b}\right)\\
w_0^* &= \sum_{m=1,3,5}^{\infty} \sum_{n=1,3,5}^{\infty} w_{0_{mn}}^* \sin\left(\tfrac{m\pi x}{a}\right) \sin\left(\tfrac{n\pi y}{b}\right)\\
\theta_x &= \sum_{m=1,3,5}^{\infty} \sum_{n=1,3,5}^{\infty} \theta_{x_{mn}} \cos\left(\tfrac{m\pi x}{a}\right) \sin\left(\tfrac{n\pi y}{b}\right)\\
\theta_x^* &= \sum_{m=1,3,5}^{\infty} \sum_{n=1,3,5}^{\infty} \theta_{x_{mn}}^* \cos\left(\tfrac{m\pi x}{a}\right) \sin\left(\tfrac{n\pi y}{b}\right)\\
\theta_y &= \sum_{m=1,3,5}^{\infty} \sum_{n=1,3,5}^{\infty} \theta_{y_{mn}} \sin\left(\tfrac{m\pi x}{a}\right) \cos\left(\tfrac{n\pi y}{b}\right)\\
\theta_y^* &= \sum_{m=1,3,5}^{\infty} \sum_{n=1,3,5}^{\infty} \theta_{y_{mn}}^* \sin\left(\tfrac{m\pi x}{a}\right) \cos\left(\tfrac{n\pi y}{b}\right)\\
\theta_z &= \sum_{m=1,3,5}^{\infty} \sum_{n=1,3,5}^{\infty} \theta_{z_{mn}} \sin\left(\tfrac{m\pi x}{a}\right) \sin\left(\tfrac{n\pi y}{b}\right)\\
\theta_z^* &= \sum_{m=1,3,5}^{\infty} \sum_{n=1,3,5}^{\infty} \theta_{z_{mn}}^* \sin\left(\tfrac{m\pi x}{a}\right) \sin\left(\tfrac{n\pi y}{b}\right)\\
q_z^+ &= \sum_{m=1,3,5}^{\infty} \sum_{n=1,3,5}^{\infty} q_{z_{mn}}^+ \sin\left(\tfrac{m\pi x}{a}\right) \sin\left(\tfrac{n\pi y}{b}\right).
\end{aligned} \tag{12}$$

and electrostatic potential is as

$$\xi(x, y, z) = \sum_{m=1,3,5}^{\infty} \sum_{n=1,3,5}^{\infty} \xi_{mn}(z) \sin\left(\frac{m\pi x}{a}\right) \sin\left(\frac{n\pi y}{b}\right).$$

The above expansions are substituted in the equilibrium equations (Eq. 11) which yield the following algebraic system of equations.

$$[X]_{12x12} \begin{Bmatrix} u_0\\ v_0\\ w_0\\ \theta_x\\ \theta_y\\ \theta_z\\ u_0^*\\ v_0^*\\ w_0^*\\ \theta_x^*\\ \theta_y^*\\ \theta_z^* \end{Bmatrix}_{12x1} = \begin{Bmatrix} 0\\ 0\\ q_z^+\\ 0\\ 0\\ (h/2)q_z^+\\ 0\\ 0\\ (h^2/4)q_z^+\\ 0\\ 0\\ (h^3/8)q_z^+ \end{Bmatrix}_{12x1} - V_t \begin{Bmatrix} V_{z1}\\ V_{z2}\\ V_{z3}\\ V_{z4}\\ V_{z5}\\ V_{z6}\\ V_{z7}\\ V_{z8}\\ V_{z9}\\ V_{z10}\\ V_{z11}\\ V_{z12} \end{Bmatrix}_{12x1}, \tag{13}$$

where $[X]$ is elastic stiffness matrix derived by Kant and Swaminathan [21]. Elements of voltage vector $\{V_{zi}\}$ are given in Appendix A. q_z^+ is the mechanical loading term and $\xi(x, y, z)$ is the electrical loading term. Through thickness electric potential $\xi_{mn}(z)$ is assumed as per the following sub-section.

2.3. Electrostatic potential

The elastic substrate is attached with distributed actuator layer of PFRC. Thickness of the PFRC layer is small as compared to thickness of the substrate. Electro-static potential in the actuator layer

Table 1
Normalized in-plane and transverse displacements $(\bar{u}, \bar{w})$ of symmetric substrate (0°/90°/0°) without and with applied sinusoidal electric voltages at top of the PFRC actuator surface.

Theory	S = 10			S = 20			S = 100		
	V = 0	V = 100	V = −100	V = 0	V = 100	V = −100	V = 0	V = 100	V = −100
$\bar{u}(0, \frac{b}{2}, \pm\frac{h}{2})$									
Present[a]	0.00632	−3.11842	3.13105	0.00617	−0.71474	0.72709	0.00613	−0.02191	0.03416
	[−4.31]	[−0.72]	[−0.73]	[−2.05]	[−1.13]	[−1.16]	[−1.20]	[−1.75]	[−1.27]
	−0.00689	0.87887	−0.89266	−0.00658	0.21675	−0.22992	−0.00648	0.00249	−0.01544
	[−1.50]	[−1.22]	[−1.23]	[−1.76]	[−2.06]	[−2.00]	[−0.37]	[−4.33]	[−1.66]
FEM[b]	0.00580	−2.82040	2.83190	0.00600	−0.69290	0.70490	0.00610	−0.02170	0.03390
	[−12.12]	[−10.21]	[−10.22]	[−4.76]	[−4.15]	[−4.17]	[−1.61]	[−2.69]	[−2.02]
	−0.00610	0.92460	−0.93680	−0.00640	0.21870	−0.23140	−0.00650	0.00240	−0.01530
	[−12.86]	[3.92]	[3.65]	[−4.48]	[−1.17]	[−1.36]	[0.00]	[−7.69]	[−2.55]
Exact[c]	0.00660	−3.14100	3.15420	0.00630	−0.72290	0.73560	0.00620	−0.02230	0.03460
	−0.00700	0.88970	−0.90380	−0.00670	0.22130	−0.23460	−0.00650	0.00260	−0.01570
$\bar{w}(\frac{a}{2}, \frac{b}{2}, 0)$									
Present[a]	−0.66806	129.05500	−130.39100	−0.47112	29.77240	−30.71460	−0.40432	0.77533	−1.58397
	[−5.91]	[−2.89]	[−2.91]	[−3.18]	[−1.86]	[−1.90]	[−1.12]	[−1.52]	[−1.31]
FEM[b]	−0.65110	122.46000	−124.70000	−0.45710	28.28700	−29.20100	−0.40220	0.76320	−1.57760
	[−8.30]	[−7.86]	[−7.15]	[−6.06]	[−6.76]	[−6.74]	[−1.64]	[−3.06]	[−1.71]
Exact[c]	−0.71000	132.90000	−134.30000	−0.48660	30.33700	−31.31000	−0.40890	0.78730	−1.60500

[a] HOSNT12.
[b] FOST based 14].
[c] Ref. [13], [% error] = 100 × (Present − Exact)/Exact.

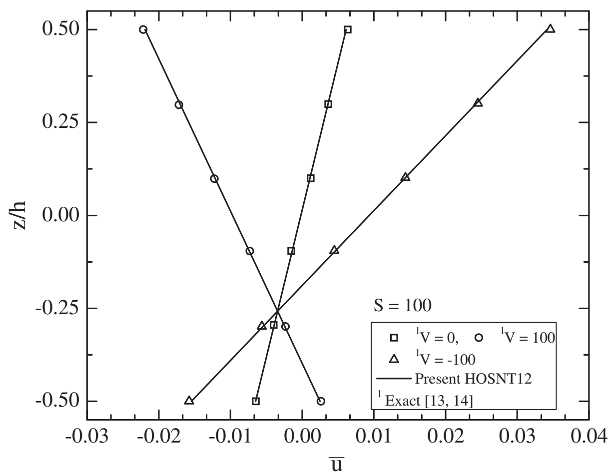

Fig. 2. Variation of normalized in-plane displacement $(\bar{u})$ through the thickness of symmetric substrate (0°/90°/0°) without and with applied sinusoidal electric voltages at top of the PFRC actuator surface.

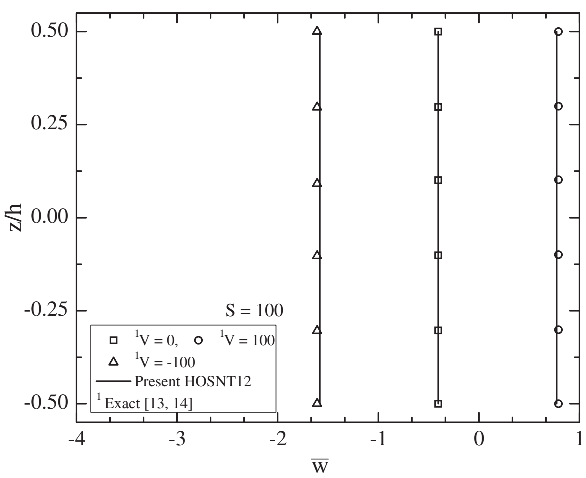

Fig. 3. Variation of normalized transverse displacement $(\bar{w})$ through the thickness of symmetric substrate (0°/90°/0°) without and with applied sinusoidal electric voltages at top of the PFRC actuator surface.

is assumed to be linear through the thickness of the PFRC layer as follows:

$$\xi_{mn}(z) = \left(\frac{V_t}{t_p}\right)z - \left(\frac{V_t h}{2t_p}\right). \qquad (14)$$

Eq. (14) represents the linear variation of through thickness electro-static potential in the PFRC layer. V_t represents the amplitude of electro-static potential applied at top of the distributed actuator layer of PFRC whereas h and t_p are the thicknesses of elastic substrate and PFRC layer respectively. Assumed electrostatic potential satisfies the zero electric potential at interface.

Piezoelectric stress vectors are calculated from second set of Eq. (7). Substituting assumed actuating electric function from Eq. (14) (when top voltage V_t is applied), piezoelectric stress resultants are evaluated from Eq. (9). Similarly elastic stress vectors and elastic stress resultants are calculated from first set of Eqs. (7) and (8) respectively. Displacement variables are obtained by solving linear algebraic equations (Eq. 13) by substituting symbolically total stress resultants $[Q\,S\,M\,N]$ from Eq. (10) in set of equilibrium equations (Eq. 11).

Transverse shearing stress (τ_{xz}, τ_{yz}) and normal stress (σ_z) are obtained by integrating the equilibrium equations (Eq. 15) of elasticity as per,

$$\tau_{xz} = -\sum_{L=1}^{n}\int_{z_L}^{z_{L+1}}\left(\frac{\partial\sigma_x}{\partial x} + \frac{\partial\tau_{xy}}{\partial y}\right)dz,$$
$$\tau_{yz} = -\sum_{L=1}^{n}\int_{z_L}^{z_{L+1}}\left(\frac{\partial\sigma_y}{\partial y} + \frac{\partial\tau_{xy}}{\partial x}\right)dz,$$
$$\sigma_z = -\sum_{L=1}^{n}\int_{z_L}^{z_{L+1}}\left(\frac{\partial\tau_{xz}}{\partial x} + \frac{\partial\tau_{yz}}{\partial y}\right)dz. \qquad (15)$$

Table 2
Normalized in-plane and transverse normal stresses ($\bar{\sigma}_x$, $\bar{\sigma}_y$, $\bar{\sigma}_z$) of symmetric substrate (0°/90°/0°) without and with applied sinusoidal electric voltages at top of the PFRC actuator surface.

Theory	*S* = 10			*S* = 20			*S* = 100		
	V = 0	*V* = 100	*V* = −100	*V* = 0	*V* = 100	*V* = −100	*V* = 0	*V* = 100	*V* = −100
$\bar{\sigma}_x(\frac{a}{2},\frac{b}{2},\pm\frac{h}{2})$									
Present[a]	−0.50746	247.54300	−248.55800	−0.49326	56.75720	−57.74370	−0.48872	1.73795	−2.71540
	[−3.91]	[−0.49]	[−0.51]	[−2.03]	[−0.89]	[−0.91]	[−1.23]	[−0.97]	[−1.06]
	0.55160	−70.76880	71.87200	0.52389	−17.41310	18.46090	0.51439	−0.20484	1.23362
	[−1.90]	[−1.25]	[−1.26]	[−1.25]	[−2.23]	[−2.19]	[−0.94]	[−6.08]	[−1.83]
FEM[b]	−0.49150	235.46000	−236.40000	−0.50220	57.26700	−58.27600	−0.49410	1.74830	−2.73640
	[−6.93]	[−5.35]	[−5.37]	[−0.26]	[0.00]	[0.00]	[−0.14]	[−0.38]	[−0.30]
	0.52150	−71.56500	72.57000	0.53040	−17.09000	18.07400	0.51210	0.21060	1.24780
	[−7.26]	[−0.14]	[−0.30]	[−0.02]	[−4.04]	[−4.24]	[−1.39]	[−196.56]	[−0.70]
Exact[c]	−0.52810	248.76000	−249.82000	−0.50350	57.26900	−58.27600	−0.49480	1.75490	−2.74450
	0.56230	−71.66600	72.79000	0.53050	−17.81000	18.87500	0.51930	−0.21810	1.25660
$\bar{\sigma}_y(\frac{a}{2},\frac{b}{2},\pm\frac{h}{6})$									
Present[a]	−0.23729	39.40750	−39.88210	−0.18114	9.95995	−10.32220	−0.16003	0.24780	−0.56786
	[−7.71]	[−7.35]	[−7.35]	[−4.71]	[−4.77]	[−4.78]	[−2.60]	[−4.54]	[−3.46]
	0.26263	−56.27130	56.79660	0.19960	−14.09780	14.49700	0.17609	−0.39707	0.74924
	[−6.17]	[−2.42]	[−2.46]	[−2.35]	[−0.44]	[−0.47]	[0.16]	[0.40]	[0.30]
FEM[b]	−0.23480	34.17500	−34.64500	−0.18490	9.88800	−10.25800	−0.16410	0.25710	−0.58070
	[−8.67]	[−19.65]	[−19.52]	[−2.74]	[−5.46]	[−5.37]	[−0.12]	[−0.96]	[−1.28]
	0.25730	−51.29500	51.80900	0.20400	−14.12500	14.52900	0.17070	−0.39260	0.74280
	[−8.07]	[−11.05]	[−11.02]	[−0.20]	[−0.25]	[−0.25]	[−2.90]	[−0.73]	[−0.56]
Exact[c]	−0.25710	42.53200	−43.04600	−0.19010	10.45900	−10.84000	−0.16430	0.25960	−0.58820
	0.27990	−57.66700	58.22700	0.20440	−14.16000	14.56600	0.17580	−0.39550	0.74700
$\bar{\sigma}_z(\frac{a}{2},\frac{b}{2},0)$									
Present[a]	−0.47467	53.72950	−54.67880	−0.47661	–	–	−0.47728	0.09546	−1.05002
	[−1.22]	[9.31]	[9.11]	[−1.81]	–	–	[−1.71]	[141.31]	[3.88]
Exact[c]	−0.48052	49.15300	−50.11400	−0.48540	1.61150	−2.58240	−0.48560	0.03956	−1.01080

[a] HOSNT12.
[b] FOST based [14].
[c] Ref. [13], [% error] = 100 × (Present − Exact)/Exact.

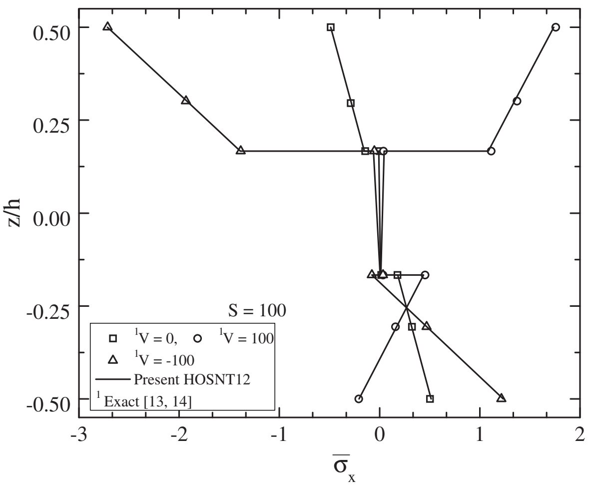

Fig. 4. Variation of normalized in-plane normal stress ($\bar{\sigma}_x$) through the thickness of symmetric substrate (0°/90°/0°) without and with applied sinusoidal electric voltages at top of the PFRC actuator surface.

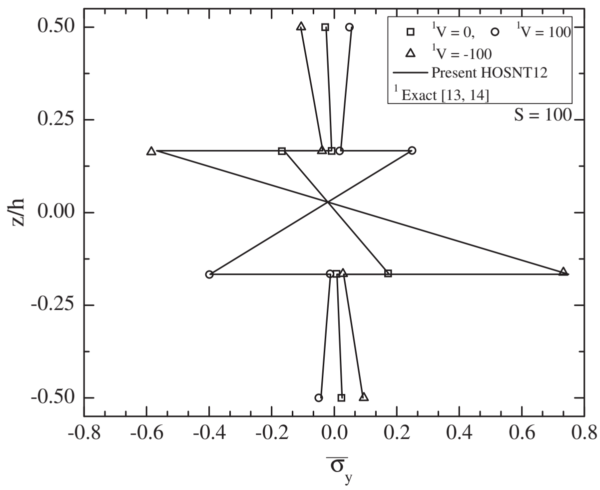

Fig. 5. Variation of normalized in-plane normal stress ($\bar{\sigma}_y$) through the thickness of symmetric substrate (0°/90°/0°) without and with applied sinusoidal electric voltages at top of the PFRC actuator surface.

3. Numerical results

A hybrid all side simply (diaphragm) supported cross ply laminates (substrate) is considered [13,14]. Substrate consists of elastic bi-directional orthotropic layers of graphite/epoxy composite. Piezoelectric material of PFRC attached at top of the elastic substrate is in a distributed form. The material properties of elastic orthotropic layers are as [13].

$$E_L = 172.9\ \text{GPa}, \quad \frac{E_L}{E_T} = 25, \quad G_{LT} = 0.5E_T, \quad G_{TT} = 0.2E_T, \quad \nu_{LT} = \nu_{TT} = 0.25, \tag{16}$$

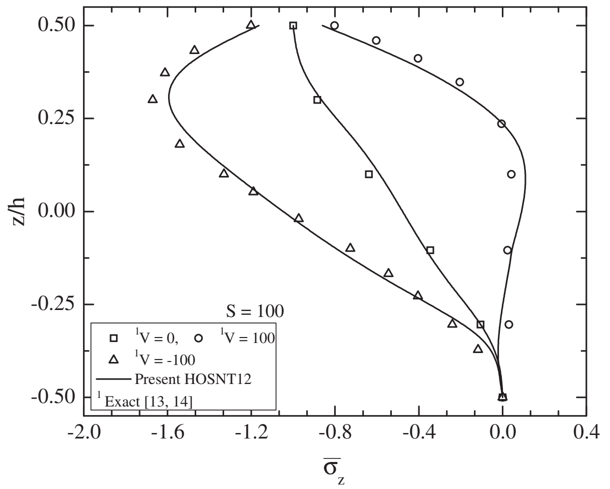

Fig. 6. Variation of normalized transverse normal stress ($\bar{\sigma}_z$) through the thickness of symmetric substrate (0°/90°/0°) without and with applied sinusoidal electric voltages at top of the PFRC actuator surface.

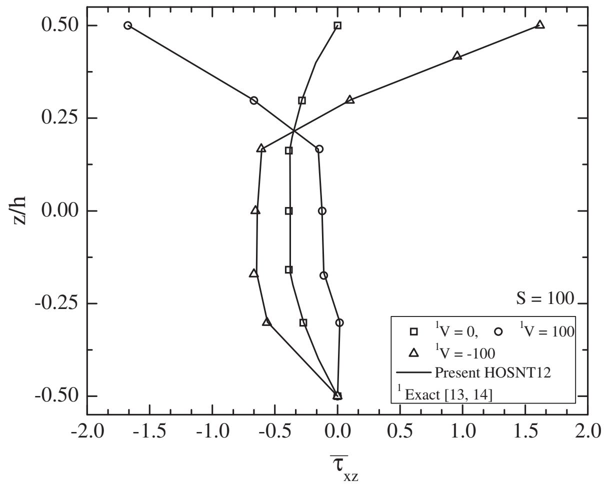

Fig. 7. Variation of normalized transverse shear stress ($\bar{\tau}_{xz}$) through the thickness of symmetric substrate (0°/90°/0°) without and with applied sinusoidal electric voltages at top of the PFRC actuator surface.

L signifies direction parallel to fiber direction and T the transverse direction.

The material properties of PFRC layer are as follows [13].

$$\begin{aligned} &C_{11} = 32.6\ \text{GPa}, \quad C_{12} = C_{21} = 4.3\ \text{GPa}, \\ &C_{13} = C_{31} = 4.76\ \text{GPa}, \quad C_{22} = C_{33} = 7.2\ \text{GPa}, \\ &C_{23} = 3.85\ \text{GPa}, \quad C_{44} = 1.05\ \text{GPa}, \quad C_{55} = C_{66} = 1.29\ \text{GPa}, \\ &e_{31} = -6.76\ \text{C/m}^2, \quad \eta_{11} = \eta_{22} = 0.037E-9\ \text{C/V m}, \\ &\eta_{33} = 10.64E-9\ \text{C/V m}. \end{aligned} \tag{17}$$

Numerical results are computed by taking $m = n = 1$.

Case i: Doubly sinusoidal mechanical load ($q_z^+ = 40\ \text{N/m}^2$, downward) without applied voltage at top of actuator ($V = 0$).

Case ii: Doubly sinusoidal mechanical load ($q_z^+ = 40\ \text{N/m}^2$, downward) with doubly sinusoidal applied voltage of positive polarity at top of actuator ($V_t = +100$ V).

Case iii: Doubly sinusoidal mechanical load ($q_z^+ = 40\ \text{N/m}^2$, downward) with doubly sinusoidal applied voltage of negative polarity at top of actuator ($V_t = -100$ V).

The above three load cases are represented by the following loads:

$$q_z^+ = \sum_{m=1,3,5}^{\infty} \sum_{n=1,3,5}^{\infty} -40 \sin\left(\frac{m\pi x}{a}\right) \sin\left(\frac{n\pi y}{b}\right) \quad \text{and}$$

$$\xi\left(x, y, \frac{h}{2} + tp\right) = \sum_{m=1,3,5}^{\infty} \sum_{n=1,3,5}^{\infty} \pm 100 \sin\left(\frac{m\pi x}{a}\right) \sin\left(\frac{n\pi y}{b}\right). \tag{18}$$

Different values for length to thickness of substrate/laminate ratios $S = a/h$ are considered. The thickness of actuator is 250 μm and that of each orthotropic layer is 1 mm. Edges ($x = 0$, a and

Table 3
Normalized in-plane and transverse shear stresses ($\bar{\tau}_{xy}$, $\bar{\tau}_{xz}$, $\bar{\tau}_{yz}$) of symmetric substrate (0°/90°/0°) without and with applied sinusoidal electric voltages at top of the PFRC actuator surface.

Theory	$S = 10$			$S = 20$			$S = 100$		
	$V = 0$	$V = 100$	$V = -100$	$V = 0$	$V = 100$	$V = -100$	$V = 0$	$V = 100$	$V = -100$
$\bar{\tau}_{xy}(0, 0, \pm\frac{h}{2})$									
Present[a]	0.02473	−7.56623	7.61569	0.02084	−1.79126	1.83293	0.01942	−0.05187	0.09071
	[−5.24]	[−1.69]	[−1.71]	[−3.09]	[−1.69]	[−1.71	[−1.43]	[−1.58]	[−1.62]
	−0.02643	4.52824	−4.58109	−0.02191	1.10547	−1.14928	−0.02028	0.02462	−0.06518
	[−4.25]	[−1.96]	[−1.99]	[−2.20]	[−1.58]	[−1.59]	[−0.59]	[−1.74]	[−1.18]
FEM[b]	0.02410	−7.00660	7.05470	0.02140	−1.81400	1.85650	0.01970	−0.05260	0.09150
	[−7.66]	[−8.96]	[−8.95]	[−0.47]	[−0.44]	[−0.45]	[0.00]	[−0.19]	[−0.76]
	−0.02510	4.24190	−4.29200	−0.02240	1.12320	−1.16790	−0.02040	0.02502	−0.06580
	[−9.06]	[−8.16]	[−8.17]	[0.00]	[0.00]	[0.00]	[0.00]	[−0.16]	[−0.24]
Exact[c]	0.02610	−7.69600	7.74800	0.02150	−1.82200	1.86480	0.01970	−0.05270	0.09220
	−0.02760	4.61900	−4.67400	−0.02240	1.12320	−1.16790	−0.02040	0.02506	−0.06596
$\bar{\tau}_{xz}(0, \frac{b}{2}, 0)$									
Present[a]	−0.35304	23.02620	−23.73220	−0.37465	–	–	−0.38249	−0.12410	−0.64088
	[2.40]	[−2.47]	[−2.33]	[−2.26]	–	–	[−0.57]	[5.67]	[−1.70]
Exact	−0.34476	23.60900	−24.29800	−0.38330	0.68194	−1.44850	−0.38470	−0.11744	−0.65197
$\bar{\tau}_{yz}(\frac{a}{2}, 0, 0)$									
Present[a]	−0.11596	23.94060	−24.17250	−0.09144	–	–	−0.08232	0.16094	−0.32558
	[−4.23]	[−0.52]	[−0.55]	[9.91]	–	–	[0.64]	[1.05]	[0.85]
Exact[c]	−0.12108	24.06500	−24.30700	−0.08320	0.88142	−1.04780	−0.08180	0.15927	−0.32284

[a] HOSNT12.
[b] FOST based [14].
[c] Ref. [13], [% error] = 100 × (Present − Exact)/Exact.

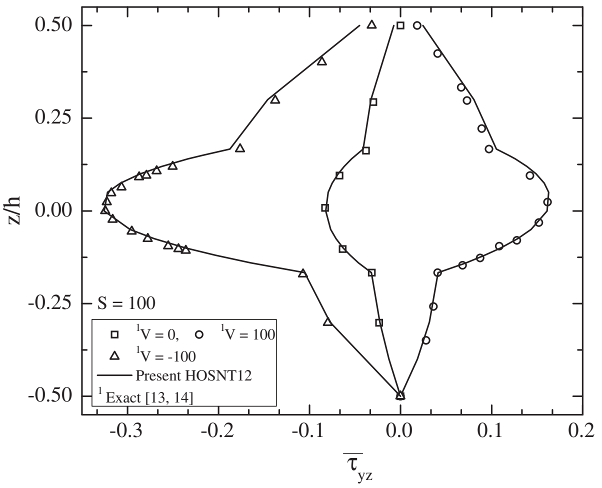

Fig. 8. Variation of normalized transverse shear stress ($\bar{\tau}_{yz}$) through the thickness of symmetric substrate (0°/90°/0°) without and with applied sinusoidal electric voltages at top of the PFRC actuator surface.

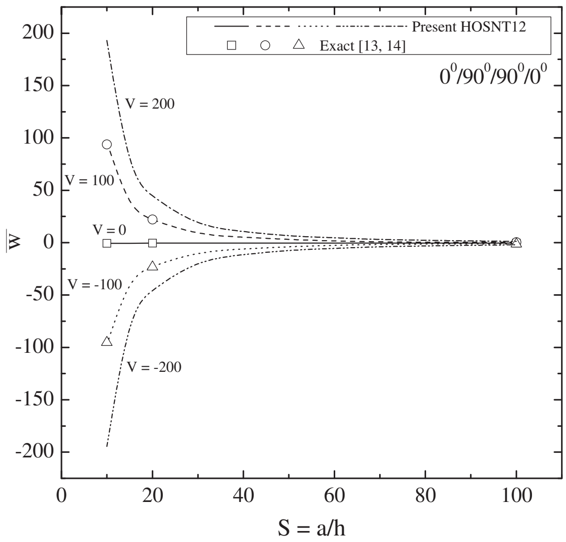

Fig. 9. Variation of normalized transverse displacement (w) with respect to aspect ratio ($S = a/h$) of symmetric substrate (0°/90°/90°/0°) without and with applied sinusoidal electric voltages at top of the PFRC actuator surface.

$y = 0$, b) of the hybrid laminate are grounded and in thickness direction also, substrate is not permitting any charge.

The results are normalized as:

$$\bar{u}\left(0,\tfrac{b}{2},\pm\tfrac{h}{2}\right) = \frac{E_2}{q_0S^3h}u, \quad \bar{w}\left(\tfrac{a}{2},\tfrac{b}{2},0\right) = \frac{100E_2}{q_0S^4h}w,$$
$$\bar{\sigma}_x\left(\tfrac{a}{2},\tfrac{b}{2},\pm\tfrac{h}{2}\right) = \frac{\sigma_x}{q_0S^2}, \quad \bar{\sigma}_y\left(\tfrac{a}{2},\tfrac{b}{2},\pm\tfrac{h}{6}\right) = \frac{\sigma_y}{q_0S^2}, \quad \bar{\sigma}_z\left(\tfrac{a}{2},\tfrac{b}{2},0\right) = \frac{\sigma_z}{q_0},$$
$$\bar{\tau}_{xy}\left(0,0,\pm\tfrac{h}{2}\right) = \frac{\tau_{xy}}{q_0S^2}, \quad \bar{\tau}_{yz}\left(\tfrac{a}{2},0,0\right) = \frac{\tau_{yz}}{q_0S}, \quad \bar{\tau}_{xz}\left(0,\tfrac{b}{2},0\right) = \frac{\tau_{xz}}{q_0S}. \tag{19}$$

E_2 is transverse Young's modulus of the elastic orthotropic layer. Three laminate configurations are taken into consideration: three layered symmetric [0°/90°/0°], four layered symmetric [0°/90°/90°/0°] and four layered antisymmetric [0°/90°/0°/90°].

Results are compared with 3D exact solution [13] and FE solution based on FOST [14].

Normalized in-plane and transverse displacements ($\bar{u}, \bar{w}$) are demonstrated for hybrid laminate [0°/90°/0°] in Table 1 subjected to mechanical pressure, positive and negative polarity voltages for various aspect ratios ($S = 10$, 20 and 100). In case of moderately thick laminate ($S = 10$) subjected to electrostatic loading (Case ii and case iii), % error in in-plane displacement ($\bar{u}$) of present HOSNT12 is up to 0.72 where as for FOST based FEM is 10.21. HOSNT12 and FEM under predict results in normalized transverse displacement ($\bar{w}$) with 2.89 and 7.15% deviation respectively. It is observed that present HOSNT12 yields most accurate results of displacement quantities as compared to FOST based FEM. Actuating voltages (Case ii and Case iii) produce in-plane displacement response ($\bar{u}$) nearly 475 times more for $S = 10$, 116 times for $S = 20$ and 5 times for $S = 100$ as compared with no voltage case (Case i). In case of transverse displacement ($\bar{w}$) the actuation response is nearly 200 times for $S = 10$ and 4 times for $S = 100$ than that of no actuation case. It is observed that the actuating voltage is more effective in case of thick laminates rather than thin. Present HOSNT12 exhibits excellent performance in all the loading cases and aspect ratios for normalized in-plane and transverse displacements ($\bar{u}, \bar{w}$) over FOST based on FEM. This is due to cubical variation in approximation of in-plane displacement as well as in transverse normal displacement components ($\bar{u}, \bar{w}$). Through thickness variations of in-plane displacements ($\bar{u}$) and transverse displacements ($\bar{w}$) are presented in Figs. 2 and 3 respectively. As far as thin plate ($S = 100$) is concerned, variations for displacements are linear and constant through the thickness of the

Table 4
Normalized in-plane and transverse displacements ($\bar{u}, \bar{w}$) of symmetric substrate (0°/90°/90°/0°) without and with applied sinusoidal electric voltages at top of the PFRC actuator surface.

Theory	$S = 10$			$S = 20$			$S = 50$			$S = 100$		
	$V = 0$	$V = 100$	$V = -100$	$V = 0$	$V = 100$	$V = -100$	$V = 0$	$V = 100$	$V = -100$	$V = 0$	$V = 100$	$V = -100$
$\bar{u}(0,\frac{b}{2},\pm\frac{h}{2})$												
Present[a]	0.0063	−2.5543	2.5669	0.0063	−0.5917	0.6042	0.0062	−0.0872	0.0997	0.0063	−0.0170	0.0295
	[−1.84]	[0.32]	[−0.09]	[−0.70]	[−0.27]	[−0.28]				[−0.74]	[−0.38]	[−0.86]
	−0.0068	0.5105	−0.5241	−0.0066	0.1097	−0.1230	−0.0066	0.0114	−0.0246	−0.0066	−0.0021	−0.0111
	[0.48]	[10.52]	[10.23]	[−0.84]	[0.83]	[0.73]				[−0.08]	[4.98]	[−0.99]
Exact[b]	0.0064	−2.5463	2.5691	0.0063	−0.5933	0.6059				0.0063	−0.0171	0.0298
	−0.0068	0.4619	−0.4755	−0.0067	0.1088	−0.1221				−0.0066	−0.0020	−0.0112
$\bar{w}(\frac{a}{2},\frac{b}{2},0)$												
Present[a]	−0.6893	96.2234	−97.6020	−0.4833	22.1061	−23.0727	−0.4210	3.1248	−3.9669	−0.4119	0.4722	−1.2961
	[−3.41]	[2.47]	[2.40]	[−1.76]	[−0.16]	[−0.23]				[−0.95]	[−1.06]	[−0.98]
Exact[b]	−0.7137	93.9010	−95.3180	−0.4920	22.1410	−23.1250				−0.4159	0.4772	−1.3089

[a] HOSNT12.
[b] Ref. [13], [% error] = 100 × (Present − Exact)/Exact.

Table 5
Normalized in-plane and transverse normal stresses $(\bar{\sigma}_x, \bar{\sigma}_y, \bar{\sigma}_z)$ of symmetric substrate (0°/90°/90°/0°) without and with applied sinusoidal electric voltages at top of the PFRC actuator surface.

Theory	S = 10			S = 20			S = 50			S = 100		
	V = 0	V = 100	V = −100	V = 0	V = 100	V = −100	V = 0	V = 100	V = −100	V = 0	V = 100	V = −100
$\bar{\sigma}_x(\frac{a}{2},\frac{b}{2},\pm\frac{h}{2})$												
Present[a]	−0.5091	205.435	−206.4530	−0.5014	47.1483	−48.1510	−0.4992	6.9249	−7.9233	−0.4989	1.3497	−2.3475
	[−0.78]	[1.95]	[1.94]	[−0.74]	[0.39]	[0.36]				[−0.95]	[−0.39]	[−0.63]
	0.5325	−31.2141	32.2792	0.5244	−8.1721	9.2209	0.5236	−0.9193	1.9667	0.5237	0.1609	0.8865
	[−2.04]	[−16.72]	[−16.30]	[−1.17]	[−7.62]	[−6.93]				[−0.01]	[4.25]	[−1.53]
Exact[b]	−0.5131	201.5000	−202.5200	−0.5051	46.9660	−47.9760				−0.5037	1.3549	−2.3624
	0.5436	−37.4800	38.5670	0.5306	−8.8460	9.9071				0.5237	0.1543	0.9002
$\bar{\sigma}_y(\frac{a}{2},\frac{b}{2},\pm\frac{h}{6})$												
Present[a]	−0.3619	44.3140	−45.0378	−0.2844	11.9512	−12.5200	−0.2571	1.7562	−2.2704	−0.2530	0.2525	−0.7584
	[−4.49]	[−4.41]	[−4.41]	[−2.61]	[−2.40]	[−2.41]				[−1.34]	[−2.15]	[−1.63]
	0.3796	−56.2092	56.9683	0.2948	−14.3787	14.9682	0.2655	−2.1208	2.6520	0.2612	−0.3370	0.8593
	[−2.84]	[1.79]	[1.72]	[1.51]	[−0.04]	[−0.11]				[−0.40]	[−0.06]	[−0.26]
Exact[b]	−0.3789	46.3580	−47.1150	−0.2920	12.2450	−12.8290				−0.2564	0.2580	−0.7709
	0.3907	−55.2210	56.0030	0.2993	−14.3850	14.9840				0.2622	−0.3372	0.8616
$\bar{\sigma}_z(\frac{a}{2},\frac{b}{2},0)$												
Present[a]	−0.4783	29.6492	−30.6059	−0.4825	7.8104	−8.7755	−0.4841	0.8849	−1.8532	−0.4844	−0.1406	−0.8283
	[−2.08]	[−0.44]	[−0.49]	[−1.62]	[7.40]	[6.33]				[−1.38]	[−21.08]	[2.98]
Exact[b]	−0.4885	29.7800	−30.7560	−0.4905	7.2723	−8.2532				−0.4912	−0.1781	−0.8043

[a] HOSNT12.
[b] Ref. [13], [% error] = 100 × (Present − Exact)/Exact.

Table 6
Normalized in-plane and transverse shear stresses $(\bar{\tau}_{xy}, \bar{\tau}_{xz}, \bar{\tau}_{yz})$ of symmetric substrate (0°/90°/90°/0°) without and with applied sinusoidal electric voltages at top of the PFRC actuator surface.

Theory	S = 10			S = 20			S = 50			S = 100		
	V = 0	V = 100	V = −100	V = 0	V = 100	V = −100	V = 0	V = 100	V = −100	V = 0	V = 100	V = −100
$\bar{\tau}_{xz}(0,\frac{b}{2},0)$												
Present[a]	−0.2983	6.9344	−7.5311	−0.3232	1.4682	−2.1145	−0.3315	−0.0475	−0.6156	−0.3329	−0.2620	−0.4038
	[0.96]	[−8.10]	[−7.44]	[−0.01]	[−6.91]	[−4.90]				[−0.40]	[0.99]	[−1.28]
Exact[b]	−0.2955	7.5453	−8.1363	−0.3232	1.5771	−2.2234				−0.3342	−0.2594	−0.4090
$\bar{\tau}_{yz}(\frac{a}{2},0,0)$												
Present[a]	−0.1878	26.1666	−26.5422	−0.1507	6.9740	−7.2754	−0.1377	1.0327	−1.3083	−0.1358	0.1580	−0.4296
	[−2.18]	[−1.51]	[−1.52	[−1.11]	[−0.38]	[−0.41]				[0.02]	[0.49]	[0.17]
Exact[b]	−0.1920	26.5680	−26.9520	−0.1524	7.0003	−7.3051				−0.1358	0.1572	−0.4289
$\bar{\tau}_{xz}(0,0,\pm\frac{h}{2})$												
Present[a]	0.0249	−5.9510	6.0009	0.0213	−1.4311	1.4737	0.0200	−0.2095	0.2497	0.0199	−0.0374	0.0772
	[−2.95]	[0.12]	[0.09]	[−1.81]	[−0.33]	[−0.37]				[−1.02]	[−0.78]	[−1.03]
	−0.0264	3.1209	−3.1738	−0.0222	0.7306	−0.7749	−0.0207	0.0989	−0.1405	−0.0206	0.0093	−0.0505
	[−1.31]	[6.09]	[5.96]	[−1.09]	[0.22]	[0.14]				[−0.52]	[−1.82]	[−0.77]
Exact[b]	0.0257	−5.9440	5.9953	0.0217	−1.4358	1.4791				0.0201	−0.0377	0.0780
	−0.0268	2.9417	−2.9952	−0.0224	0.7290	−0.7738				−0.0207	0.0095	−0.0509

[a] HOSNT12.
[b] Ref. [13], [% error] = 100 × (Present − Exact)/Exact.

laminate for in-plane displacement $(\bar{u})$ and transverse displacement $(\bar{w})$ respectively.

Results for normalized in-plane and transverse normal stresses $(\bar{\sigma}_x, \bar{\sigma}_y, \bar{\sigma}_z)$ are tabulated in Table 2 under the loading cases *i*, *ii*, and *iii* and aspect ratios 10, 20 and 100. Response of in-plane normal stress $(\bar{\sigma}_x)$ is nearly three times more than that of in-plane normal stress$(\bar{\sigma}_y)$ for $S = 10$. Present HOSNT12 values are within 3.91% while the FOST based FEM values are within 6.93% less than exact values. Transverse normal stress values with present HOSNT12 deviate by 9.31% for aspect ratio 10. Variations in normalized in-plane and transverse normal stresses $(\bar{\sigma}_x, \bar{\sigma}_y, \bar{\sigma}_z)$ are presented in Figs. 4–6 respectively under the loading cases *i*, *ii*, and *iii* and aspect ratio 100. Piezoelectric stress coefficient is effective only in *x* direction (e_{31}) and $e_{32} = 0$, in-plane normal stress$(\bar{\sigma}_y)$ in top layer is less actuated than top layer in, in-plane normal stress$(\bar{\sigma}_x)$. Present HOSNT12 is seen to predict accurately the variations in normalized in-plane and transverse normal stresses $(\bar{\sigma}_x, \bar{\sigma}_y, \bar{\sigma}_z)$. Normalized in-plane and transverse shear stresses $(\bar{\tau}_{xy}, \bar{\tau}_{xz}, \bar{\tau}_{yz})$ are presented in Table 3. Here again the HOSNT12 predicts very accurate results of transverse shear stress $(\bar{\tau}_{xz}, \bar{\tau}_{yz})$ quantities with marginal 2.47% and 0.52% errors respectively. Variations of transverse shear stresses $(\bar{\tau}_{xz}, \bar{\tau}_{yz})$ are plotted in Figs. 7 and 8.

Results of four layered laminated composite [0°/90°/90°/0°] are shown in Table 4. For a moderately thick laminate ($S = 10$), present HOSTN12 over predicts the in-plane displacement quantity $(\bar{u})$ by 0.32% only at top ($z = +h/2$) for load Case *ii*. Maximum deviation in

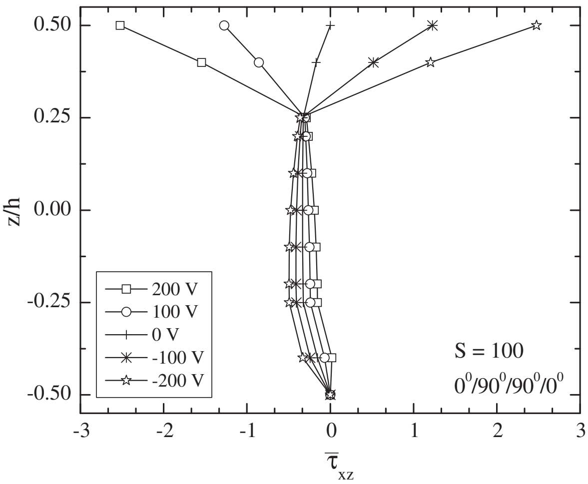

Fig. 10. Normalized transverse shear stress (τ_{xz}) across the thickness of symmetric substrate (0°/90°/90°/0°) without and with applied sinusoidal electric voltages at top of the PFRC actuator surface.

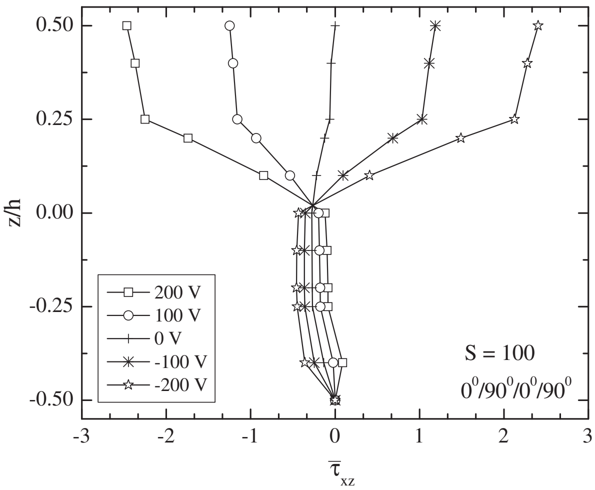

Fig. 11. Normalized transverse shear stress (τ_{xz}) across the thickness of antisymmetric substrate (0/90°/0°/90°) without and with applied sinusoidal electric voltages at top of the PFRC actuator surface.

transverse displacement is up to marginal 2.47% for load cases *ii* and *iii*. Variation of transverse displacement ($\bar{w}$) with respect to aspect ratio ($S = a/h$) of four layered symmetric substrate without and with applied sinusoidal electric voltages at top of the PFRC actuator surface is presented in Fig. 9. Effect of actuation is effective in case of thick than thin laminates. In Table 5, normalized in-plane and transverse normal stresses ($\bar{\sigma}_x, \bar{\sigma}_y, \bar{\sigma}_z$) are presented. Present HOSNT12 yields accurate results for transverse normal stress ($\bar{\sigma}_z$)

Table 7
Normalized displacements and stresses for antisymmetric substrate (0°/90°/0°/90°) without and with applied sinusoidal electric voltages at top of the PFRC actuator surface.

Theory	S = 10			S = 20			S = 50			S = 100		
	V = 0	V = 100	V = −100	V = 0	V = 100	V = −100	V = 0	V = 100	V = −100	V = 0	V = 100	V = −100
$\bar{u}(0,\frac{b}{2},\pm\frac{h}{2})$												
Present[a]	0.00971	−4.73418	4.7536	0.00910	−0.92249	0.92948	0.00891	−0.12662	0.14445	0.00890	−0.02449	0.04227
	[−6.64]	[−7.34]	[−7.34]	[−3.16]	[−2.90]	[−4.05]				[−1.11]	[−1.24]	[−1.25]
	−0.00614	0.83670	−0.8489	−0.00593	0.15559	−0.16124	−0.00587	0.01753	−0.02928	−0.00590	−0.00010	−0.01163
	[−2.60]	[7.89]	[7.71]	[−1.14]	[−1.15]	[−4.82]				[0.00]	[−100.56]	[−1.48]
FEM[b]	0.00920	−4.53640	4.5643	0.00890	−0.85580	0.87350				0.00890	−0.02420	0.04190
	[−11.54]	[−11.21]	[−11.03]	[−5.32]	[−9.92]	[−9.83]				[−1.11]	[−2.42]	[−2.10]
	−0.00590	0.93350	−0.9452	−0.00590	0.16260	−0.17440				−0.00590	0.01790	−0.01150
	[−6.35]	[20.37]	[19.92]	[−1.67]	[3.30]	[2.95]				[0.00	[−2.19]	[−2.54]
Exact[c]	0.01040	−5.10940	5.1301	0.00940	−0.95000	0.96870				0.00900	−0.02480	0.04280
	−0.00630	0.77550	−0.7882	−0.00600	0.15740	−0.16940				−0.00590	0.01830	−0.01180
$\bar{w}(\frac{a}{2},\frac{b}{2},0)$												
Present[a]	−0.65578	146.4720	−147.7830	−0.51616	31.94070	−32.36550	−0.4767	4.51912	−5.47252	−0.47082	0.77082	−1.71292
	[−8.12]	[−0.86]	[−0.93]	[−3.54]	[−1.37]	[−3.25]				[−1.17]	[−1.40]	[−1.25]
FEM[b]	−0.66430	131.9700	−131.6800	−0.51020	30.14200	−31.16300				−0.46940	0.75840	−1.69700
	[−6.92]	[−10.68]	[−11.72]	[−4.65]	[−6.92]	[−6.85]				[−1.47]	[−2.99]	[−2.17]
Exact[c]	−0.71370	147.7500	−149.1700	−0.53510	32.38300	−33.45300				−0.47640	0.78180	−1.73460
$\bar{\sigma}_z(\frac{a}{2},\frac{b}{2},0)$												
Present[a]	−0.4706	59.0357	−59.9769	−0.4737	16.1618	−17.1091	−0.4748	2.2859	−3.2356	−0.4750	0.0500	−1.1690
	[−2.00]	[3.95]	[3.85]	[−2.08]	[21.58]	[19.97]				[−2.06]	[0.00]	[14.60]
Exact[c]	−0.4802	56.7920	−57.7520	−0.48375	13.2930	−14.2610				−0.4850	0.0500	−1.0200
$\bar{\tau}_{xz}(0,\frac{b}{2},0)$												
Present[a]	−0.2708	15.1892	−15.7308	−0.2740	2.2260	−2.7739	−0.2749	0.0511	−0.6010	−0.2751	−0.1963	−0.3538
	[2.45]	[−5.79]	[−5.53]	[0.34]	[−11.54]	[−9.43]				[−0.37]	[1.47]	[−1.33]
Exact[c]	−0.2643	16.1230	−16.6520	−0.27305	2.5165	−3.0626				−0.2761	−0.1935	−0.3586
$\bar{\tau}_{yz}(\frac{a}{2},0,0)$												
Present[a]	−0.2597	55.3315	−55.8510	−0.2632	16.2201	−16.7464	−0.2642	2.5110	−3.0393	−0.2643	0.4347	−0.9632
	[1.18]	[1.22]	[1.22]	[0.00]	[0.75]	[0.73]				[−0.38]	[−0.51]	[−0.45]
Exact[c]	−0.2567	54.6630	−55.1760	−0.26315	16.0990	−16.6250				−0.2653	0.4369	−0.9676

[a] HOSNT12.
[b] FOST based [14].
[c] Ref. [13], [% error] = 100 × (Present − Exact)/Exact.

values under load case *ii* and $S = 10$ with a maximum % error of 0.49 only. New results are presented for $S = 50$ and are in tune with other results. Normalized in-plane and transverse shear stresses $(\bar{\tau}_{xy}, \bar{\tau}_{xz}, \bar{\tau}_{yz})$ are presented in Table 6. Present HOSNT12 predicts these shear stresses accurately with maximum 8.10% error in $(\bar{\tau}_{xy})$, 2.18% in $(\bar{\tau}_{xz})$ and 6.09% in $(\bar{\tau}_{yz})$. Normalized variation in transverse shear stress $(\bar{\tau}_{xz})$ is presented in Fig. 10 to demonstrate actuating effects on the laminate. As observed earlier, top layer of laminate [0°/90°/90°/0°] is affected maximum due to actuation along *x*-direction for $S = 100$.

Next, antisymmetric laminate configuration [0°/90°/0°/90°] is considered under electromechanical loading. Normalized displacements and stresses are presented in Table 7. Maximum error of 7.89% is observed for HOSNT12 as compare to 20.37% error in FOST based FEM for in-plane displacement $(\bar{u})$ for moderately thick laminate ($S = 10$). Differences for transverse displacement $(\bar{w})$ are 0.93% and 11.72%. In transverse shear stresses $(\bar{\tau}_{xz}, \bar{\tau}_{yz})$, % error is observed to be 5.79 and 1.22 respectively for HOSNT12 and FEM. Normalized variation of transverse shear stress $(\bar{\tau}_{xz})$ across the thickness of antisymmetric substrate is displayed in Fig. 11. Top two layers [90°] and [0°] are largely affected due to actuating potentials as compared to bottom layers [90°] and [0°].

4. Conclusions

In this paper a complete analytical solution for statics of laminates attached with distributed PFRC actuator under electromechanical loading is presented. A higher order shear and normal deformation theory is used to model the elastic responses of laminate subjected to voltages. Linear layer wise (LW) approximation of the electrostatic potential proposed in the present model is simple to model and gives accurate results. Comparative numerical results for across the thickness variations of displacements and stresses are presented. Linear and constant variations of in-plane and transverse displacements are observed. Actuating effects are more in case of thick than thin laminates. Considerable effects of actuation at the interfaces are observed in case of in-plane normal stresses and transverse shear stresses along *x*-axis as compared to their effects along *y*-axis. It can be concluded that the present HOSNT12 model is accurate and more reliable compared to FOST based FEM. Shear and normal deformation effects are very significant at interface of actuator and laminate and cannot be ignored while modeling laminates, especially under electromechanical loading.

Appendix A

$$V_{z1} = \frac{e_{31}\pi}{a}, \quad V_{z2} = \frac{e_{32}\pi}{b}, \quad V_{z3} = -\frac{(b^2 e_{15} + a^2 e_{24})\pi^2 t_p}{2a^2 b^2},$$

$$V_{z4} = -\frac{\pi(-e_{15}t_p + e_{31}(h + t_p))}{2a}, \quad V_{z5} = -\frac{\pi(-e_{24}t_p + e_{32}(h + t_p))}{2a},$$

$$V_{z6} = -\frac{\left(-b^2 e_{15}\pi^2 t_p(3h + 4t_p) + a^2\left(12b^2 e_{33} + e_{24}\pi^2 t_p(3h + 4t_p)\right)\right)}{12a^2 b^2},$$

$$V_{z7} = -\frac{\pi\left(-2e_{15}t_p(3h + 4t_p) + e_{31}(3h^2 + 6ht_p + 4t_{tp}^2)\right)}{12a},$$

$$V_{z8} = -\frac{\pi\left(-2e_{24}t_p(3h + 4t_p) + e_{32}(3h^2 + 6ht_p + 4t_{tp}^2)\right)}{12b},$$

$$V_{z9} = \frac{1}{24}\left(24e_{33}(h + t_p) - \frac{(b^2 e_{15} + a^2 e_{24})\pi^2 t_p(3h^2 + 8ht_p + 6t_p^2)}{a^2 b^2}\right),$$

$$V_{z10} = \frac{\pi\left(-8e_{15}t_{tp}^2(3h^2 + 8ht_p + 6t_{tp}^2) + e_{31}\left(-h^4 + (h + 2t_p)^4\right)\right)}{64at_p},$$

$$V_{z11} = \frac{\pi\left(-8e_{24}t_{tp}^2(3h^2 + 8ht_p + 6t_{tp}^2) + e_{32}\left(-h^4 + (h + 2t_p)^4\right)\right)}{64bt_p},$$

$$V_{z12} = \frac{1}{80}\left(-20e_{33}(3h^2 + 6ht_p + 4t_p^2) - \frac{(b^2 e_{15} + a^2 e_{24})\pi^2 t_p(5h^3 + 20h^2 t_p + 30ht_p^2 + 16t_p^2)}{a^2 b^2}\right).$$

References

[1] Tiersten HF, Mindlin RD. Forced vibrations of piezoelectric crystal plates. Quart Appl Math 1962;20:107–19.
[2] Tiersten HF. Linear piezoelectric plate vibrations. New York: Plenum Press; 1969.
[3] Mallik N, Ray MC. Effective coefficients of piezoelectric fiber reinforced composites. AIAA J 2003;41(4):704–10.
[4] Robbins DH, Reddy JN. Analysis of piezoelectrically actuated beams using a layer-wise displacement theory. Comput Struct 1991;41(2):265–79.
[5] Tauchert TR. Plane piezothermoelastic response of a hybrid laminate – a benchmark problem. Compos Struct 1997;39(3-4):329–36.
[6] Chandrashekhara K, Agarwal A. Active vibration control of laminated composite plates using piezoelectric devices-a finite element approach. J Intel Mater Syst Struct 1993;4(4):496–508.
[7] Saravanos DA, Heyliger PR, Hopkins DA. Layerwise mechanics and finite element for the dynamic analysis of piezoelectric composite plates. Int J Solids Struct 1997;34(3):359–78.
[8] Kapuria S, Kulkarni SD. An efficient quadrilateral element based on improved zigzag theory for dynamic analysis of hybrid plates with electroded piezoelectric actuators and sensors. J Sound Vib 2008;315(1-2):118–45.
[9] Ballhause D, D'Ottavio M, Kröplin B, Carrera E. A unified formulation to assess multilayered theories for piezoelectric plates. Comput Struct 2005;83(15-16):1217–35.
[10] Mannini A, Gaudenzi P. Multi-layer higher-order finite elements for the analysis of free-edge stresses in piezoelectric actuated laminates. Compos Struct 2004;63(3-4):263–70.
[11] Wu L, Jiang Z, Feng W. An analytical solution for static analysis of a simply supported moderately thick sandwich piezoelectric plate. Struct Eng Mech 2004;17(5):641–54.
[12] Ray MC, Bhattacharya R, Samanta B. Exact Solutions for static analysis of intelligent structures. AIAA J 1993;31:1684–91.
[13] Mallik N, Ray MC. Exact solutions for the analysis of piezoelectric fiber reinforced composites as distributed actuators for smart composite plates. Int J Mech Mater Des 2004;1:347–64.
[14] Ray MC, Mallik N. Finite element analysis of smart structures containing piezoelectric fiber reinforced composite actuator. AIAA J 2004;42(7):1398–405.
[15] Heyliger P. Static behavior of laminated elastic/piezoelectric plates. AIAA J 1994;32:2481–4.
[16] Vel SS, Batra RC. Three-dimensional analytical solution for hybrid multilayered piezoelectric plates. ASME J Appl Mech 2000;67:558–67.
[17] Kant T. Numerical analysis of thick plates. Comput Methods Appl Mech Eng 1982;31:1–18.
[18] Kant T, Owen D, Zinkiewicz OC. A refined higher-order C° plate bending element. Comput Struct 1982;15:177–83.
[19] Pandya BN, Kant T. A consistent refined theory for flexure of a symmetric laminate. Mech Res Commun 1987;14:107–13.
[20] Kant T, Manjunatha BS. An unsymmetric FRC laminate C° finite element model with 12 degrees of freedom per node. Eng Comput 1988;5:300–8.
[21] Kant T, Swaminathan K. Analytical solutions for the static analysis of laminated composite and sandwich plates based on a higher order refined theory. Compos Struct 2002;56:329–44.